Paleohydraulic reconstruction of a 40 kyr-old terrace sequence implies that water discharge was larger than today*

Camille Litty[1], Robert Duller[2], Fritz Schlunegger[1]
[1] *Institute of Geological Sciences, University of Bern, Baltzerstrasse, 1+3, CH- 3012 Bern.*
[2] *Department of Earth, Ocean & Ecological Sciences, School of Environmental Sciences, University of Liverpool, 4 Brownlow Street, Liverpool, L69 3GP.*

Abstract

The evolution of landscapes crucially depends on the climate history. This is particularly evident in South America where landscape responses to orbital climate shifts have been well documented. However, while most studies have focused on inferring temperature variations from paleoclimate proxy data, estimates of water budget changes have been complicated because of a lack of adequate physical information. Here, we present a methodology and related results, which allowed us to extract water discharge values from the sedimentary record of the 40 Ka-old fluvial terrace deposits in the Pisco valley, western Peru. In particular, this valley hosts a Quaternary cut-and-fill succession that we used, in combination with 10Be-based sediment flux, gauging records, channel geometries and grain size measurements, to quantitatively assess sediment and water discharge values c. 40 Ka ago in relation to present-day conditions. We compare these discharge estimates to the discharge regime of the modern Pisco River and find that the water discharge of the paleo-Pisco River, during the Minchin pluvial period c. 40 Ka ago, was c. 7-8 times greater than the modern Pisco River if considering the mean and the maximum water discharge. In addition, the calculations show that inferred water discharge estimates are mainly dependent on channel gradients and grain size values, and to a lesser extent on channel width measures. Finally, we found that the c. 40 Ka-old Minchin terrace material was poorer sorted than the modern deposits, which might reflect that sediment transport during the past period was characterized by a larger divergence from equal mobility compared to the modern situation. In summary, the differences in grain size distribution and inferred water discharge estimates between the modern and the paleo-Pisco River suggests that the 40 Ka-old Minchin period was characterized by a wetter climate and more powerful flood events.

Keywords: *Paleohydraulic reconstructions, grain size, water discharge, climate change, Pisco valley, Peru*

Introduction

Fluvial and hillslope processes are the primary mechanisms by which sediments are transported from mountainous terrains to depositional basins. The sensitivity of river process to changes in tectonic and climatic boundary conditions makes fluvial successions an ideal archive, if fragmentary, from which past changes in these boundary conditions can be inferred (Heller and Paola, 1992; Whipple, 2004; Church, 2006; Allen, 2008). However, inversion of these is non-trivial because tectonics and climate have a similar net impact on surface elevation change, mediated by river processes (Humphrey and Heller, 1995). In this context, many interpretations particularly in terms of climate change scenarios have been developed from the observation of models because natural, well-preserved sediment deposits are rare.

Here, we focus on the Quaternary cut-and-fill terrace sequences in the Pisco valley (Figure 1), located on the western Andean margin at 13°S, where the results of previous chronological (Steffen et al., 2009) and ^{10}Be-based investigations (McPhillips et al., 2013; Bekaddour et al., 2014) provide ideal datasets that can be utilized to explore the controls on the sedimentary processes preserved by the terraces and the modern deposits. In this valley, sediment supply and transport during the past 40 kyrs has been related to orbital shifts in paleoclimate (Bekaddour et al., 2014) and seismicity (McPhillips et al., 2014). The main arguments for interpretation of these mechanisms were based on: (i) populations of ^{10}Be concentrations encountered in pebbles and boulders, that were considered to reflect the erosional response to seismicity patterns (McPhilipps et al., 2014), (ii) ^{10}Be-based sediment fluxes that were used to infer changes in precipitation rates and regimes (Bekaddour et al., 2014; McPhilipps et al. 2013), and (iii) the temporal coincidence between pluvial periods on the Altiplano and sedimentation in the Pisco valley, based on stratigraphic investigations of the terrace material (Steffen et al., 2009). Despite these results, interpretations of whether or not changes in water discharge have taken place are ambiguous due to lack of physical evidence. This physical evidence for past water discharge is embedded in the sediments and formative dimensions of the channel (Church, 2006). Using sedimentary, specifically sediment caliber, and morphometric information from the 54-34 ka-old terrace sequences in the Pisco valley (Steffen et al., 2009; Figure 1) we reconstruct past water discharge (Church, 2002; 2006; Duller et al., 2012) and compare this hydraulic information to that of the modern river to demonstrate differences, or not, between the two time periods. Our study provides new field data to constrain, and to test, possible impacts of climatic changes on the characteristics of fluvial deposits and to quantify the magnitude of these changes.

Geomorphological setting

The c. 200 km-long Pisco River is sourced from the Pultoc Lake on the Altiplano of central Peru (c. 5000 m.a.s.l.) and its course runs across the western Andean Escarpment before joining the Pacific Ocean near Pisco at 13°S (Figure 1). During the late Miocene, there was a phase of surface uplift of the Altiplano and of the western Andean slope, the vestiges of which are still visible in the shape of the modern river profile (Schildgen et al., 2007). The long stream profile is characterized by two segments separated by a c. 20 km-long knickzone at c. 120 km distance from the coast. The bedrock is composed of Tertiary volcaniclastic deposits in the upstream segments, Late Jurassic and Early Cretaceous sediments in the middle segment, and a Cretaceous to early Tertiary Batholith in the lower segment (inset of Figure 1; Davila, 1993; INGEMENT, 2011). Upstream of the knickzone where Tertiary volcaniclastic deposits are found, bedrock is exposed on the channel floor, while a deeply-incised channel floor composed of mixed bedrock and alluvial cover characterizes the knickzone (Abbühl et al., 2011). In the knickzone, the channel is c. 50 m wide whereas farther downstream to the Pacific coast, the valley widens to several hundreds of meters, and the channel is composed of an alluvial cover. This alluvial cover (or river bed material) is made up of rounded polygenic pebbles and sand (Figures 2E-F).

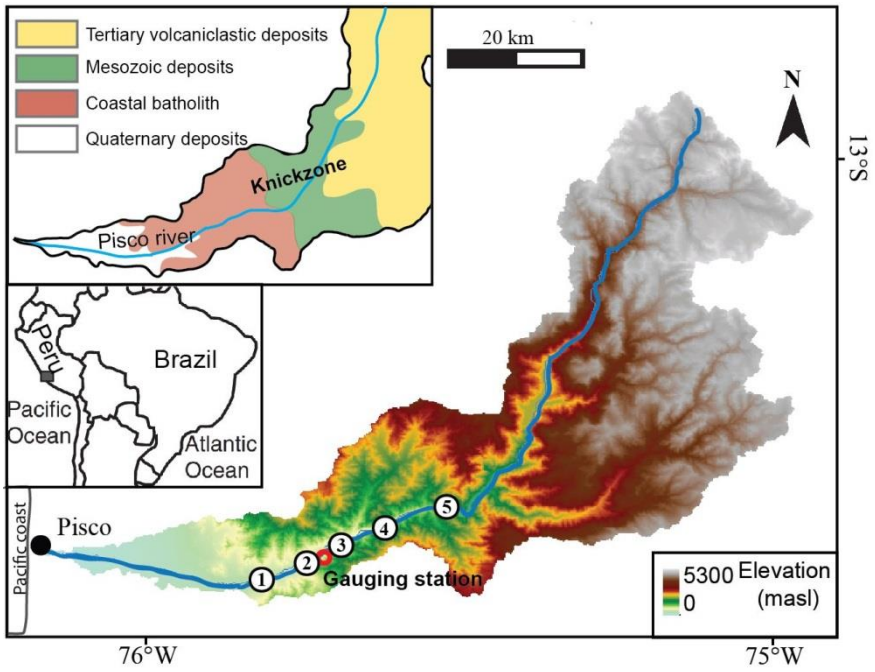

Figure 1: *Elevation map of the Pisco River drainage basin, which is based on Shuttle Radar Topography Mission 90 m data. Inset in the upper left corner shows a simplified geological map of the study area (modified from INGEMENT, 2011 and Bekaddour et al., 2014). Circles represent sites where grain size data have been collected.*

Quaternary cut-and-fill terrace sequences are common features along other rivers that occur along the coastal margin between Peru and northern Chile. The Pisco drainage basin (4300 km^2) (Figure 1) hosts three, well-preserved Quaternary terrace levels. The terrace sequences have been dated to 54-34 ka for terrace level T1 and to 26-15 ka for level T2 using optically stimulated luminescence (OSL) dating techniques (Steffen et al., 2009; Trauerstein et al., 2014). The T2 terrace level (Steffen et al., 2009) is only preserved in few places. We focus on the well-preserved terrace level T1 (e.g., Figure 2A), which is referred to as the Minchin terrace (Steffen et al., 2009) as its construction was coeval with the Minchin palaeolake on the Altiplano when rainfall rates were supposedly higher than at present (Baker et al., 2001a, 2001b; Placzek et al., 2006). This terrace level is made up of a >50 meter-thick sequence with predominantly clast-supported horizontally stratified conglomerates (e.g., Figures 2C and 3), of mixed composition, at the base that were deposited by the Pisco trunk stream during this time (Steffen et al., 2009). Towards the top of the sequences, matrix-supported breccias, of monomict composition, become more frequent and make up the uppermost units of most of these sequences, mainly in the upstream part of the valley (Figure 4). The occurrence of these deposits suggests the supply of material by debris flows from tributary valleys, constructing lateral fans that were prograding into the valley axis through time as the terrace sequence was built up (Steffen et al., 2009).

The Minchin terrace level can be identified for 40 km along the entire valley floor from the onset of the knickzone to within 30 km of the Pacific coast (Figure 4; Steffen et al., 2009). Accordingly, the chronological framework of polymict fluvial deposits preserved in the terrace sequences (implying the transport by the Pisco trunk stream) in combination with the present river bed material in the Pisco valley provide conditions to assess the physical signature of the inferred climate changes within the fluvial material. In particular, we test whether a higher water discharge for the Pisco River during the Minchin pluvial period has to be invoked to explain the transport of T1 material during this time. We also explore whether differences in climates between the Minchin period and today explains the

contrasts in the characteristics of the fluvial deposits, particularly in terms of the grain size distribution.

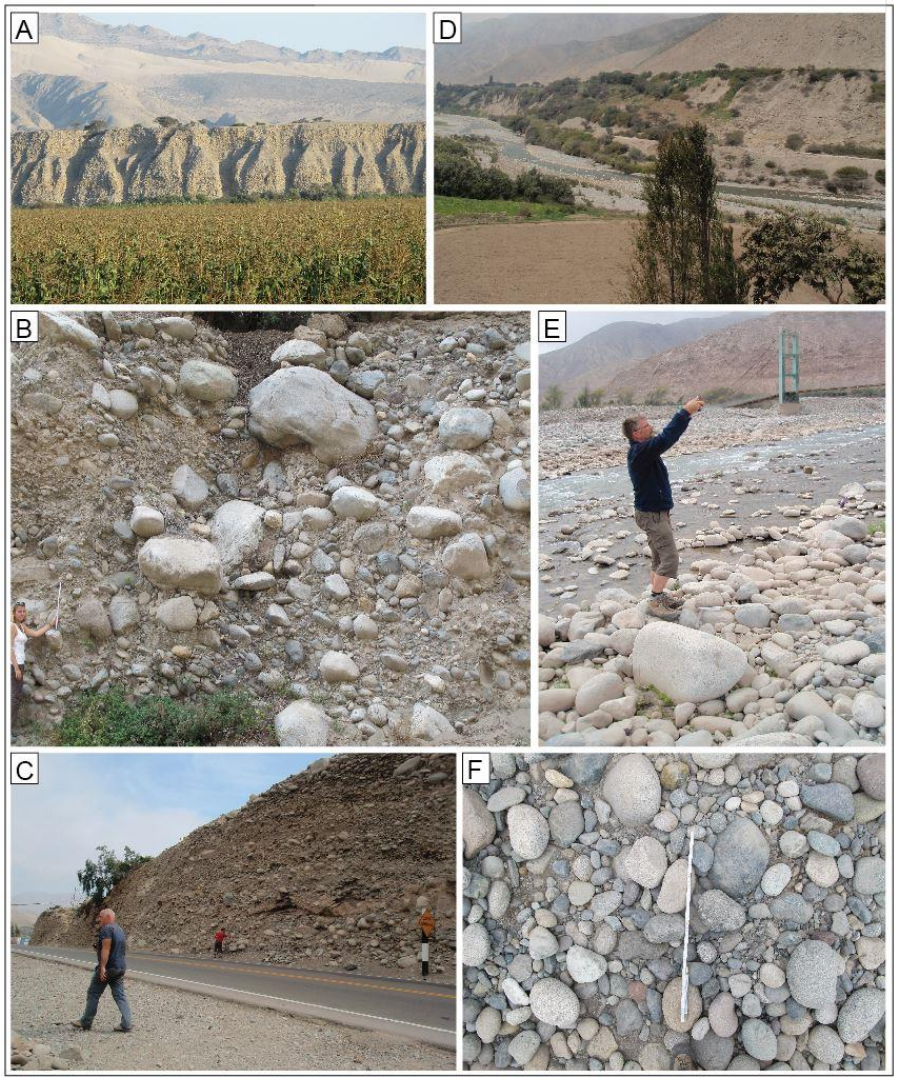

Figure 2: *(A) View looking to the south toward the Minchin terrace escarpment from the present Pisco River belt. (B) Photo of the terrace deposits taken north of sampling site 5. Meter-scale boulders and centimeter-scale pebbles are distinguishable. (C) View looking to the north toward sampling site 2. The photo illustrates the Minchin sediments. Meter-scale boulders are rare. (D) Picture illustrating the present Pisco River at site 2. The modern river belt and the Minchin terrace deposits (background) are visible. (E) View to the northeast, showing person who takes photos of sampling site 5. (F) Modern deposits depicted at sampling site 2.*

Methods

According to these scopes, we proceeded by measuring: (i) the grain size distributions along the Pisco River collected from digital images. These were taken from modern longitudinal stream bars and from well-exposed and accessible outcrops of the Minchin terrace deposits; (ii) the flow strengths and related water discharges for the two time periods, using the Bagnold equation for sediment transport (e.g. Tucker and Slingerland, 1997) and published ^{10}Be-based sediment budgets as basis (Bekaddour et al., 2014) that will be corrected for solute and suspension loads. Flow strength and

water discharge estimates additionally require information about the morphometric properties of the stream including channel gradients and widths during the Minchin time and the present-day. Accordingly, we mapped the terrace deposits in the field, on satellite images and on the 90 m resolution DEM.

As mentioned above, in the upper reaches at >50 km upstream from the river mouth, the Minchin deposits comprise fluvial gravels at the base (clast supported, polymict gravels exhibiting imbrication in places) and debris flow units (matrix supported, monomict breccias) at the top in most sections (Figure 4C; Steffen et al., 2009). This suggests that while the lateral supply of sediment has been accomplished through debris flow processes, the down-valley transport of this material occurred principally through fluvial transport mechanisms (Steffen et al., 2009). Towards the coast, however, the Minchin deposits are exclusively made up of fluvial gravels, implying that the valley fill comprises river-lain material (Figure 4C, Steffen et al., 2009). As the equations used in this paper (see below) are designed for fluvial and not debris flow processes, we will focus our hydrological analyses mainly on the lower reach and on fluvial gravels only.

Grain size data

We determined the grain size of river sediments at 5 sites (Figures 1A, 2) along the 120 km-long reach downstream of the knickzone where both present channel bar and Minchin terrace deposits were accessible. Grain size data was collected from imbricated and horizontally-stratified, clast-supported conglomerates of fluvial origin (Steffen et al., 2009; Figures 2 and 4C). At each site, the *b*-axis of particles were measured from digital images that were taken at 5 to 7 different locations within an area of circa 200 m^2 (modern stream) and within 10 m of vertical section (Minchin terrace). Sites of the Minchin terrace were selected to represent the identical chronological level (within errors) of c. 5 ka (Figure 4C; Steffen et al., 2009). This strategy yielded a total of c. 2500 grain size measurements per site for the modern material, and c. 4000 per site for the terrace deposits. These numbers of measurements have been considered as sufficient for reliable estimations of the grain size distributions (e.g. Rice and Church 1998). The comparison between the grain sizes of the surface and terrace material requires correction for the modern bed material, because post depositional winnowing tends to coarsen the sediment surface (Andrews, 1984). In the same sense, Kellerhals and Bray (1971) demonstrated that areal samples tend to be biased in favor of the coarser grains, as outlined by Diplas and Fripp (1991). To solve this problem, we followed the results by Andrews (1984) who showed that surface samples are coarser up to a factor of 3 compared with the grain size distribution of the embedded sediments (Andrews, 1984). We thus account for this bias following the latter author (i.e. lowering by a factor of 3), which, however, could potentially result in an underestimate, and thus in a conservative assessment, of the role of water discharge to entrain the modern sediments.

We used the grain sizes of the 50^{th} and 96^{th} percentile values (D_{50} and D_{96}) and calculated the standard deviation of the D_{50} and D_{96} from the 5 to 7 locations at each site. The principal limitation to defining the entire grain size distribution was the inability to accurately measure particles <3 mm in diameter from digital images (see also Whittaker et al., 2010). While we cannot resolve this problem with available techniques, we do not expect that this adds a substantial bias in the grain size distributions reported here because their relative contributions to the point-count results are minor (i.e. < 5%, based on visual inspection of the digital images).

Water discharge estimates

The water discharge of the Pisco River has been surveyed during the past fifty years by the hydrological service of Peru. We thus have access to the hydrological data from a gauging station (Figure 1) located between our survey sites 2 and 3 (Agteca, 2010, Bekaddour et al., 2014; Figures 1

and 2). In addition, sediment fluxes Q_s have been estimated near the site of the gauging station using concentrations of in-situ ^{10}Be for modern and Minchin river-born sediments (Bekaddour et al., 2014), which we took here as basis to solve the Bagnold equation for the evacuation of the supplied sediment (Equation 1). According to this equation, the occurrence of sediment transport at a rate Q_s requires that critical (threshold) conditions for the mobilization of a population of gravel clasts or particles are exceeded. There are several possibilities to calculate sediment transport but all share the form of a power function of excess shear stress imparted on a river-bed. Here, we selected the Bagnold equation (e.g. Tucker and Slingerland, 1997), which relates sediment flux *Qs* (here based on the ^{10}Be-based sediment discharge estimates of Bekaddour et al., 2014) to threshold conditions for sediment entrainment and water flow strength through:

$$Q_s = \frac{aW}{(p_s - p)p^{1/2}g}(\tau - \tau_C)\left(\tau^{1/2} - \tau_c^{1/2}\right) \quad (1),$$

where W is channel width, ρ_s = 2700 kg/m^3 and ρ = 1000 kg/m^3 are sediment and water densities, respectively, τ is the shear stress exerted by water, τ_c is the critical shear stress required to entrain a sediment particle size of size D_x (with x representing the percentile) and a is a constant. We will discuss later that a depends on the effects related to skin friction and the nature of bed forms, at least in our case.

While the ^{10}Be-derived sediment discharge considers the total loads that also include the solute and suspension load components (von Blanckenburg, 2005), the Bagnold equation (eq. 1) has been derived for the bedload material only. Datasets from modern examples show that dissolved and suspended sediment loads commonly account for 50-80% of the total sediment discharge (e.g. Schlunegger and Hinderer, 2003; Hinderer et al., 2014). Accordingly, the sediment flux data of Bekaddour et al. (2014) was corrected assuming that 20-50% of the total sediment flux was bedload sediment flux. This correction yields bedload flux values of c. 16000-40000 m^3/yr (mean, 28000 m^3/yr) for the modern Pisco River, and c. 130000-325000 m^3/yr (mean, 227000 m^3/yr) for the Pisco River during the Minchin period.

We note that these fluxes have been measured on sand material that is commonly trapped in the pore space of gravels. However, the entrainment of the sand fraction in the pore spaces requires that the gravels are shifted, which occurs when minimum flow strengths are exceeded. Using D_{50} and D_{96} as threshold criteria for the entrainment of material, we are confident that the combined 10Be dataset, sediment sampling procedure and sediment transport relationships are reasonably well captured by the corrected bedload flux values given above.. In principle, this approach returns water discharge values required to evacuate the supplied bedload material (based on ^{10}Be measurements, corrected for solute and suspension components), provided that sediment transport can be accomplished during mean (threshold water strength set by the D_{50}) or peak runoff only (threshold set by the D_{96}).

For the D_{50}, we determined values of 1.2 cm ± 0.2 cm for the present and 2 cm ± 0.8 cm for the terrace deposits, while sizes of 6 cm ± 2 cm (present material) and 11.5 cm ± 4 cm (terrace deposits) were determined for the D_{96}. We obtained these measures at the locations (between sites 2 and 3) where the ^{10}Be-based sediment flux (Bekaddour et al., 2014) has been estimated, and where the Minchin terrace deposits are made up of fluvial material.

Critical shear stress values τ_c (see Equation 1) for the entrainment of the D_{50} and D_{96} can be obtained through Shields (1936) criteria, whereby a dimensionless critical shear stress τ^*_{cDx} is used to denote threshold of motion of the grain size of interest D_x:

$$\tau *_{cDx} = \frac{\tau_{cDx}}{(\rho_s - \rho) g D_x} \quad (2),$$

where ρ_s and ρ denote the particle and the water densities respectively, and g the gravitational acceleration. Shields (1936) showed that for near-uniform grains, represented best by the D_{50}, τ^*_{cDx} attains a constant value of c. 0.06 in the case of rough turbulent flow over narrowly graded sediment beds coarser than sand. Following Meyer-Müller (1948), Heller and Paola (1992) used a value of 0.047, which yields lower discharge estimates for mean water flux. However, since this will not change our conclusions regarding the contrasts in runoff between modern and past times, we applied the original value of 0.06 (Shields, 1936). This then yields the following relationships (use of D_{50}):

$$\tau_{cD50} = 0.06(\rho_s - \rho) g D_{50} \quad (3).$$

Studies dealing with non-uniform mixture of grains (e.g. Egiazaroff, 1965; Parker et al., 1982; Andrews, 1983) point to the importance of the hiding/protrusion effect or divergence from equal mobility on the critical Shields parameter, which will be lower if the coarse grained fraction of a river bed is considered. Reported values (Buffington and Montgomery, 1997 and references therein) of related Shields parameters vary considerably. According to Church (2002), however, a value of 0.03 appears a conventional approach for individual, well-exposed gravel, cobble or boulder clasts, consistent with the D_{96} selected here. In support of this statement, a relatively detailed study in an Alpine torrent returned a value of c. 0.03 (van den Berg and Schlunegger, 2012). We are thus left with either a conservative approach where the Shields variable equals 0.06, yielding an upper bound for estimating water discharge, and 0.03 returning lower water discharge values. We therefore selected a *mean* value of 0.045 as a start (see in Tables 1 and 2) and iteratively changed to values of 0.03 and 0.06, thereby exploring the sensitivity of this variable. This then yields the following relationships (use of D_{96}):

$$\tau_{cD96} = 0.045(\rho_s - \rho) g D_{96} \quad (4).$$

Bed shear stress exerted by water (see equation 1) is computed through:

$$\tau = \rho g R S \quad (5),$$

where R is the hydraulic radius, g is gravitational acceleration, S the channel gradient if steady-uniform flow is assumed, and ρ the density of water. Note by using the S term as mentioned here, equation (5) might yield in overestimations for shear stress. Accordingly, the value of the variable τ needs to exceed the threshold τ_{cDx} to entrain the grain size with the *b*-axis D_x. The hydraulic radius R is the ratio between the cross-sectional area of a flow $A\ (L^2)$ and the wetted perimeter $P\ (L)$: $R = A/P$. For wide channels where the width W of the active channel is at least twenty times larger than water depth d, it follows that $R \approx d$ (Tucker and Slingerland, 1997). Our own observation during a low discharge period (November 2014) has shown that this is the case (d<0.5 m, W≈15-25 m).

The most robust way for solving equation (5) utilizes the Darcy-Weisbach friction factor f since this variable approximates a drag coefficient if resistance is defined as the gravitational driving force per unit area and assumed to be proportional to the square of the flow velocity V (Ferguson, 2007):

$$\tau = \rho V^2 \frac{f}{8} \quad (6).$$

Values of f differ considerably between shallow- and deep-water flows and depend on grain size D relative to water depth d. Ferguson (2007) combined these relationships to a single equation referred as the *Variable-Power Equation (VPE)* where roughness-layer and skin friction effects are considered (Ferguson, 2007):

$$\frac{f}{8} = (D/d)^2 / a_2^2 + (D/d)^{1/3} / a_1^2 \quad (7),$$

where D is the grain size under consideration, d is water depth, and a_1 and a_2 are constants that vary between 7-8 and 1-4, respectively (Ferguson, 2007). The *VPE*-approach thus combines friction differences under deep and shallow flow conditions, but has the disadvantage that the related coefficients a_1 and particularly a_2 have relatively large uncertainties. However, we are faced with the problem that the Bagnold equation has too many unknowns to properly be solved with the *Variable-Power Equation*. In particular, a solution of equation (1) through the combination of equations (5), (6) and (7), and thus via the consideration of f, requires that either flow velocity V or water depth d are independently constrained, for which we lack the required datasets. We therefore selected a different approach where we solved the Bagnold equation through a combination of equation (5) and formulas describing the continuity of mass (equation 8), and Jarrett's (1984) approximation for the relationship between flow velocity and channel bed roughness (equation 9):

$$Q = VWd \quad (8),$$

and

$$V = 3.10 R^{0.83} S^{0.12} \quad (9).$$

As for equation (5), we substituted $R \approx d$, where d is the channel depth.

Although Jarrett's (1984) approximation uses high slope as a surrogate for coarse bed material, which is a simplification, we justify our solution because Marcus et al. (1992) showed that the Jarrett (1984) method yields a solid estimate for flow resistance for channel gradients <0.183, which is the case for the Pisco River.

This then returns a measure for water flow strength as a function of water discharge Q and channel width W:

$$\tau = 0.54 \rho g \left(\frac{Q}{W}\right)^{0.55} S^{0.93} \quad (10).$$

This leaves us with Q as the only non-constrained variable with analytical techniques.

We iteratively changed water discharge Q until the calculated sediment discharge Q_s equals the measured one (Table 1). We started from the modern situation, assigned the measured mean values to the input parameters (mean grain size, mean channel width etc.) and computed the corresponding water discharge solutions. We then calibrated the model with the hydrological records from a gauging station located at 52 km from the Pacific coast through adjustments of the value for the parameter a (equation 1). In addition, we explored the range of possible solutions for water

discharge values where the entire range of grain size and channel width estimates was considered. We also performed simple sensitivity analyses, thereby starting from the calibrated model (labeled as *standard* in Table 1). When then either doubled or halved the constraining variables (gradient, channel width, and grain size, Table 1) while solving the Bagnold Equation for water discharge. We finally applied our calibrated model to the situation for the Minchin times (Table 2), where we used the corresponding grain size and sediment flux data as input parameters. In summary, these calculations yielded water discharge values that are required to evacuate the known value of the supplied sediment, assuming that sediment transport can be accomplished during mean (threshold water strength set by the D_{50}) or peak runoff only (threshold set by the D_{96}).

Table I. Data used for the calculation of water discharge for the present times and water discharge calculations

	Latitude (d.d.)	Longitude (d.d.)	Elevation (m)	Gradient (m/m)	D_{50} (cm)	D_{96} (cm)	Mean channel width (m)	Maximum channel 1width (m)								
	13.65 S	75.73 W	3500	0.011	1.1 ± 0.1	7.5 ± 1.5	20 ± 5	60 ± 10								
	Low discharge pattern															
	Bagnold equation not yet calibrated with measured water flux, i.e. a = 1															
	D50 (m)		Gradient		Q = water discharge (m^3/s)		Channel width (m)	a	Shields variable	τ_c	τ	Q_s	Q_s (year)	Q_s (measured)		a = 1
Min	0.01		0.011		1.5		15	1.00	0.06	10.0	22.0	0.00052236	16473	16000–40000		Water discharge range: 1–4 m^3/s
	0.012		0.011		2		15	1.00	0.06	12.0	25.8	0.00063255	19948			
	0.01		0.011		3		25	1.00	0.06	10.0	24.3	0.00120285	37933			
Max	0.012		0.011		3.5		25	1.00	0.06	12.0	26.5	0.00115501	36425			
Mean	0.011		0.011		2.5		20	1.00	0.06	11.0	24.9	0.0008802	27759	mean Q_s: 28000		Mean water discharge: 2.5 m^3/s
	Bagnold equation calibrated with measured water flux, yielding a = 1/20															
	D50 (m)		Gradient		Q = water discharge (m^3/s)		Channel width (m)	a	Shields variable	τ_c	τ	Q_s	Q_s (year)	Q_s (measured)		a = 1/20
Min	0.01		0.011		15		15	0.05	0.06	10.0	78.1	0.00054976	17337	16000	–40000	Water discharge range: 15–35 m^3/s
	0.012		0.011		20		15	0.05	0.06	12.0	91.5	0.00068983	21755			
	0.01		0.011		30		25	0.05	0.06	10.0	86.4	0.00110935	34985			
Max	0.012		0.011		35		25	0.05	0.06	12.0	94.0	0.00121083	38185			
Mean	0.011		0.011		25		20	0.05	0.06	11.0	88.3	0.0008914	28111	mean Q_s: c. 28000		Mean water discharge: 25 m^3/s
	High discharge pattern															
	Bagnold equation not yet calibrated with measured water flux, i.e. a = 1															
	D96 (m)		Gradient		Q = water discharge (m^3/s)		Channel width (m)	a	Shields variable	τ_c	τ	Q_s	Q_s (year)	Q_s (measured)		a = 1
Min	0.06		0.011		12		40	1.00	0.03	30.0	40.3	0.00067644	21332	16000	–40000	Water discharge range: 12–100 m^3/s
	0.06		0.011		35		40	1.00	0.06	60.0	72.6	0.00073451	23163			
	0.06		0.011		17		60	1.00	0.03	30.0	39.0	0.00078986	24909			
	0.06		0.011		50		60	1.00	0.06	60.0	70.7	0.00079573	25094			
	0.09		0.011		20		40	1.00	0.03	45.0	53.4	0.00037552	11843			
	0.09		0.011		70		40	1.00	0.06	90.1	106.3	0.00100792	31786			
	0.09		0.011		30		60	1.00	0.03	45.0	53.4	0.00056329	17764			
Max	0.09		0.011		100		60	1.00	0.06	90.1	103.5	0.00104002	32798			
Mean	0.075		0.011		40		50	1.00	0.045	56.3	68.6	0.00091404	28825	mean Q_s: c. 28000		Mean water discharge: 40 m^3/s

(Continues)

Table 1. (Continued)

	Latitude (d.d.)	Longitude (d.d.)	Elevation (m)	Gradient (m/m)	D_{50} (cm)	D_{96} (cm)	Mean channel width (m)	Maximum channel 1width (m)								
	Bagnold equation calibrated with measured water flux, yielding a = 1/5															
	D96 (m)		Gradient		Q = water discharge (m^3/s)		Channel width (m)	a	Shields variable	τ_c	τ	Q_s	Q_s (year)	Q_s (measured)		a = 1/5
Min	0.06		0.011		18		40	0.20	0.03	30.0	50.4	0.00049884	15731	16000	–40000	Water discharge range: 18–150 m^3/s
	0.06		0.011		53		40	0.20	0.06	60.0	90.7	0.00082696	26079			
	0.06		0.011		26		60	0.20	0.03	30.0	48.8	0.00064363	20298			
	0.06		0.011		75		60	0.20	0.06	60.0	88.3	0.00106164	33480			
	0.09		0.011		30		40	0.20	0.03	45.0	66.7	0.00047841	15087			
	0.09		0.011		105		40	0.20	0.06	90.1	132.8	0.00132053	41644			
	0.09		0.011		45		60	0.20	0.03	45.0	66.7	0.00071761	22630			
Max	0.09		0.011		150		60	0.20	0.06	90.1	129.3	0.00168072	53003			
Mean	0.075		0.011		60		50	0.20	0.045	56.3	86.4	0.0010212	32205		mean Q_s: c. 28000	Mean water discharge: 60 m^3/s
	Sensitivity analyses for low discharge pattern															
	D50 (m)		Gradient		Q = water discharge (m^3/s)		Channel width (m)	a	Shields variable	τ_c	τ	Q_s	Q_s (year)		mean Q_s: c. 28000	
Standard	0.011		0.011		25		20	0.05	0.06	11.0	88.3	0.00089139	28111			
Half of S	0.01		0.005		100		20	0.05	0.06	10.0	90.6	0.0009708	30615			
Double of S	0.01		0.022		8		20	0.05	0.06	10.0	90.2	0.00096382	30395			
Half of W	0.01		0.011		24		7.5	0.05	0.06	10.0	148.1	0.00088453	27894			
Double of W	0.01		0.011		26		30	0.05	0.06	10.0	72.2	0.00094373	29761			
Half of D_{50}	0.005		0.011		20		15	0.05	0.06	5.0	91.5	0.00090174	28437			
Double of D_{50}	0.022		0.011		34		15	0.05	0.06	22.0	122.5	0.00091159	28748			
	Sensitivity analyses for high discharge pattern															
	D96 (m)		Gradient		Q = water discharge (m^3/s)		Channel width (m)	a	Shields variable	τ_c	τ	Q_s	Q_s (year)		mean Q_s: c. 28000 a=1/20	
Standard	0.075		0.011		60		50	0.20	0.045	56.3	86.4	0.00102122	32205			
Half of S	0.075		0.005		230		50	0.20	0.045	56.3	86.5	0.00103156	32531			
Double of S	0.075		0.022		18		50	0.20	0.045	56.3	85.2	0.00094447	29785			
Half of W	0.075		0.011		40		25	0.20	0.045	56.3	101.2	0.0010875	34295			
Double of W	0.075		0.011		100		100	0.20	0.045	56.3	78.1	0.00110654	34896			
Half of D_{50}	0.038		0.011		25		50	0.20	0.045	28.1	53.4	0.00095612	30152			
Double of D_{50}	0.150		0.011		158		50	0.20	0.045	112.6	147.1	0.00099394	31345			

Note: We estimated the water discharge for the two sites where Bekaddour et al. (2014) have calculated sediment flux from ^{10}Be-based catchment-averaged denudation rates. Beryllium-10 (^{10}Be) concentrations of modern and terrace stream material have been used to document a yearly-averaged sediment flux of c. 80 000 m^3/yr for the modern times (^{10}Be sampling site c. 10 km upstream of the gauging station) (Bekaddouret al., 2014). Datasets from modern examples show that dissolved and suspended sediment loads commonly account for 50 to 80% of the total sediment discharge. We thus corrected the sediment flux data by Bekaddour et al. (2014) thereby considering that 20–50% of the total sediment flux has been accomplished as bedload, which accounts to a flux (Q_s measured) of c. 16 000 –40 000 m^3/yr for the modern time. Q_s = sediment flux (in m^3/yr). We applied a density ρ_s = 2700 kg/m^3 for sediment particles.

Table II. Data used for the calculation of water discharge for the Minchin times and water discharge calculations

	Latitude (d.d.)	Longitude (d.d.)	Elevation (m)	Gradient (m/m)	D_{50} (cm)	D_{96} (cm)	Mean channel width (m)	Maximum channel width (m)							
	13.62 S	75.57 W	2200	0.015	2 ± 0.8	12 ± 3	180 ± 30	365 ± 65							
	Low discharge pattern														
	D50 (m)		Gradient		Q = water discharge (m^3/s)		Channel width	a	Shields variable	τ_c	τ	Q_s	Q_s (year)	Q_s (measured)	a = 0.05
Min	0.012		0.015		75		150	0.05	0.06	12.0	71.3	0.0041992	132427	130000–325000	Water discharge range: 75–300 m^3/s
	0.028		0.015		150		150	0.05	0.06	28.0	104.4	0.0053496	168703		
	0.012		0.015		120		210	0.05	0.06	12.0	76.7	0.0068248	215226		
Max	0.028		0.015		300		210	0.05	0.06	28.0	127.0	0.0117838	371614		
Mean	0.022		0.015		180		180	0.05	0.06	22.0	104.4	0.007769	245017	mean Q_s: c. 227000	Mean water discharge: 180 m^3/s
	High discharge pattern														
	D96 (m)		Gradient		Q = water discharge (m^3/s)		Channel width	a	Shields variable	τ_c	τ	Q_s	Q_s (year)	Q_s (measured)	a = 0.02
Min	0.09		0.015		180		300	0.20	0.03	45.0	78.8	0.0083388	262973	130000–325000	Water discharge range: 130–1300 m^3/s
	0.09		0.015		390		300	0.20	0.06	90.1	120.6	0.0051876	163596		
	0.09		0.015		182		430	0.20	0.03	45.0	65.1	0.0044303	139712		
	0.09		0.015		520		430	0.20	0.06	90.1	115.9	0.0053793	169643		
	0.15		0.015		286		300	0.20	0.03	75.0	101.7	0.0043091	135892		
	0.15		0.015		910		300	0.20	0.06	150.1	192.2	0.0077259	243644		
	0.15		0.015		390		430	0.20	0.03	75.0	98.9	0.0050039	157804		
Max	0.15		0.015		1300		430	0.20	0.06	150.1	191.9	0.010895	343585		
Mean	0.12		0.015		490		365	0.20	0.045	90.1	122.8	0.007197	226976	mean Q_s: 227000	Mean water discharge: 490 m^3/s

Note: We used the calibrated Bagnold model where a = 1/20 where the D_{50} sets the boundary conditions for sediment entrainment, and a = 1/5 where the D_{96} is used as constraints. As for the modern times, we applied a density $\rho_s = 2700$ kg/m^3 for sediment particles. Beryllium-10 (^{10}Be) concentrations of terrace stream material have been used to document a yearly-averaged sediment flux of c. 640 000 m^3/yr for the time when sedimentation of the Minchin deposits occurred (^{10}Be sampling site c. 5 km downstream of the gauging station) (Bekaddouret al., 2014). Datasets from modern examples show that dissolved and suspended sediment loads commonly account for 50 to 80% of the total sediment discharge. We thus corrected the sediment flux data by Bekaddour et al. (2014), which accounts to a flux (Q_s measured) of c. 130 000 –325 000 m^3/yr for the time when the Minchin material accumulated.

Terrace mapping and estimates of paleo-channel gradients and paleo-channel widths

The most important parameters in the discharge reconstruction are the longitudinal slope and channel width (see equations above). Among these, channel gradients have a larger effect as our simple sensitivity study shows (Table 1). In support of our observations, Ryder and Church (1986) have shown that paleo-hydraulic reconstructions based on terrace material are extremely sensitive to these data. The morphometric properties of the modern Pisco River were quantified through available remote sensed datasets and digital elevation models. For older, 'stratigraphic', periods, these parameters were determined using a reconstruction of the paleo-channel profile. We proceeded by mapping (Figure 3) the surface of the Minchin terrace deposits on Google Earth satellite images and on the 90 m DEM (*ASTER GDEM,* NASA), which enabled the reconstruction of the paleo-channel profile by correlating points of known altitudes and by assuming no subsequent surface tilting (Figures 4A and B). The interpolation of the elevation of these deposits is then served as basis for the calculation of the paleo-channel gradients. We note that the top of the Minchin level is made up by fluvial deposits along the lower reaches, debris flow fan material (>55 km distance from the river mouth), or a combination of both (between 40-55 km distance from the river mouth). The consideration of lateral fan material in the reconstruction of the paleo gradients could thus result in a slight overestimation of the paleo-gradients, with the effect that the calculated differences in flow strengths between present and past times will yield conservative contrasts, which is the scope here.

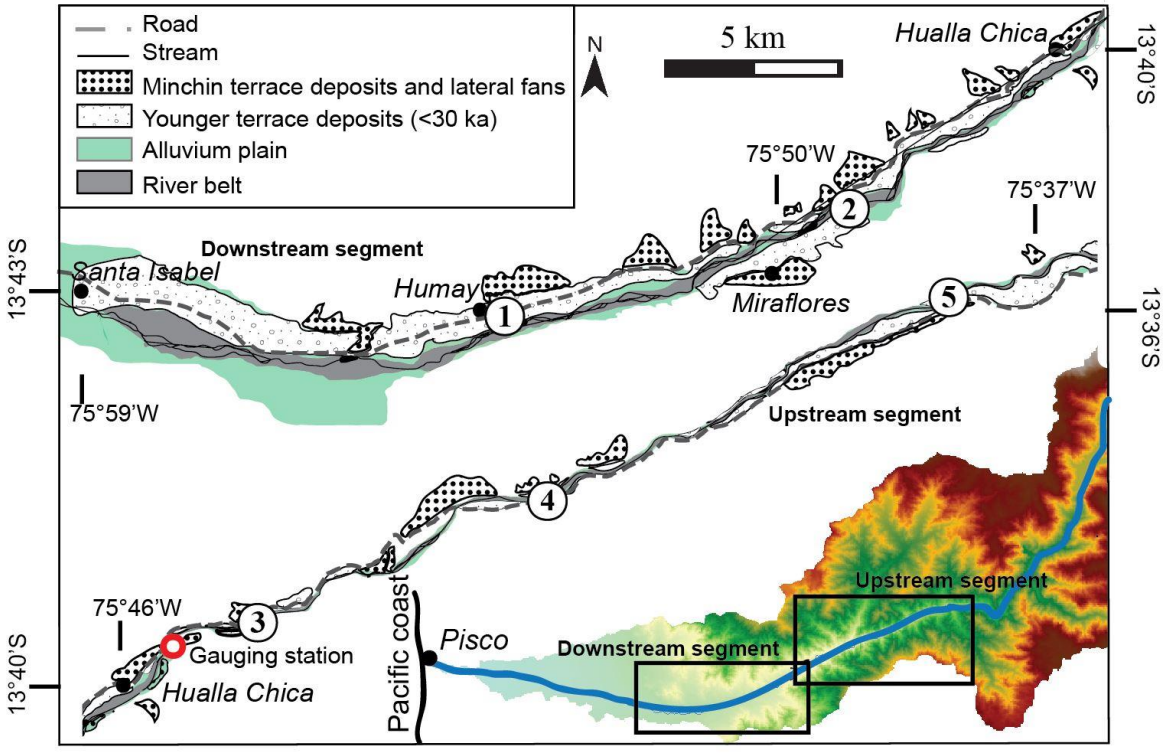

Figure 3: *Map of the occurrence of the Minchin terrace and lateral fans along the Pisco river. The map shows the location of the sampling sites for grain size data (circles) and of the gauging station.*

Mapping also serves as basis to estimate channel widths. We acknowledge that uncertainties in channel width estimates introduce errors in our calculations (Equation 1, and results of sensitivity analyses shown in Table 1). For the current situation, three variables can be readily extracted from available archives. These comprise: (i) the width of the river belt and (ii) the width of the active channel during low (dry season) and (iii) high water stages (wet season). We do have satellite images

from different years covering the river length for both periods (Figure 5), which we use here to constrain channel widths for inferring water fluxes for the entrainment of sediment during dry (mean active channel c. 20±5 m wide) and flood stages (mean active channel c. 50±10 m wide, Figures 5 and 6A). These values are nearly constant along the entire stream length and correspond to ca. 1/3 and 2/3 of the river belt width values measured between gauging station and farther upstream.

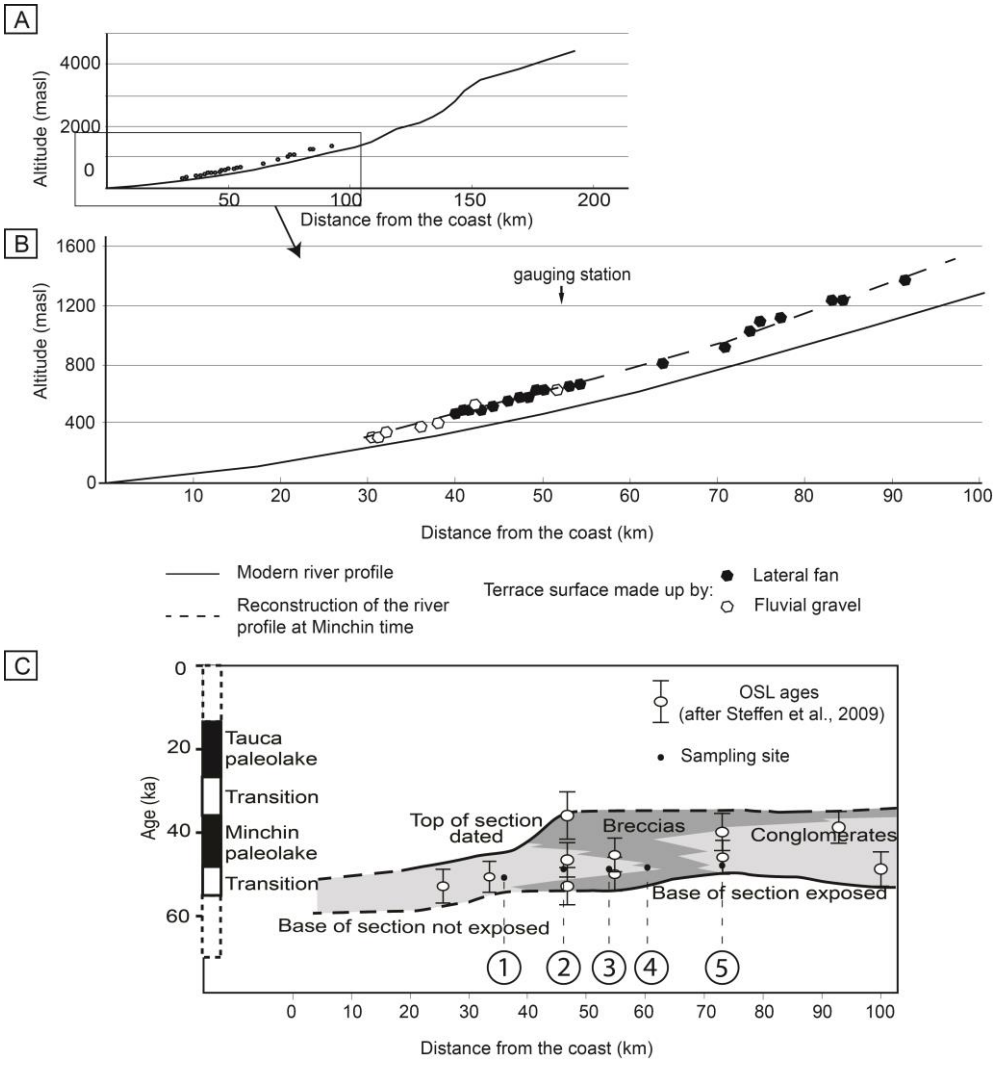

Figure 4: *(A) Pisco river profile. (B) Zoom of the figure 4A showing the altitude of the top of the terrace and of the lateral fans from which we reconstruct the river profile at the Minchin time. (C) Wheeler diagram showing the composition of the terrace level T1 along the Pisco river (modified from Steffen et al., 2009). Site numbering as in Figure 1.*

While we have no constraints on these variables for the Minchin times, we are capable of measuring values for the river belt during this period (Figure 6B), which is the cross-sectional width of the Pisco valley at the base of the terrace deposits where the material is made up of fluvial gravels (Steffen et al., 2009, see above). Similar to the present state, we anticipate the occurrence of same ratios between 1/3 and 2/3 between river belt and active channel widths for mean and high water stages in our calculations for the past. Also according to the current situation, we applied these ratios to the river belt width values that we measured at the gauging station and farther upstream, and we infer that the width of the active channel was nearly stationary along the entire Pisco River (as it is

today). As a consequence, for our site of interest between 45 and 55 km distance of the river mouth (which is the reach surrounding the gauging station), the river belt width is c. 550±100 m. Our approach thus yields an active channel width of 180 ± 30 m during low flow stages and 365 ± 65 m during high flow stages. We note that uncertainties in active channel widths will be greatest for lower flood stages since we cannot reconstruct the proportion of channel width that was occupied by water, and therefore sediment discharge. It is fair to assume that the maximum flood stages will occupy most, if not all, of the channel width when the coarsest material (D_{96}) can be mobilized. Even if this was not the case, the larger sediment fluxes, coarser grain sizes and nearly identical channel gradients during the past do call for more water during Minchin times irrespective of channel width assignments (see below). In addition, as we do not consider bankfull discharge even for the entrainment of the D_{96}, our water discharge estimates, based on equation (1), will return conservative values.

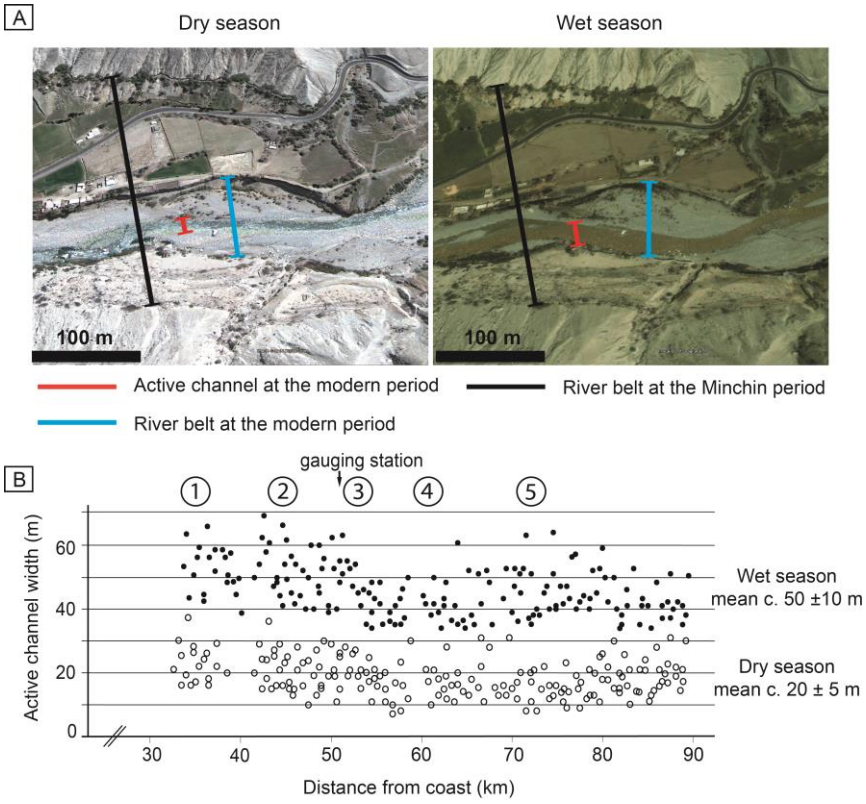

Figure 5: *(A) Satellite images showing how the active modern channel width and both the modern and the Minchin river belt widths have been measured during dry and wet season. (B) Active channel widths during wet and dry season obtained from satellite images from different years.*

Results

Terrace mapping and estimates of paleo-channel gradient

The first terrace material that we assigned to the Minchin time period has been encountered at an upstream distance of c. 90-100 km from the coast (Figure 3). From there, we mapped the highest terrace deposits c. 15 km farther downstream, where they reach an elevation of at least 80 m above the current river levels. From this location downward, relative terrace elevations decrease to 40 m, and then to 20 m at 35 km from the coast. No terrace deposits are present near the Pacific coast (Figures 3 and 4).

If we take the top terrace level as reference, then the reconstruction of the terrace surface implies a stream profile, prior to dissection by the modern river, which was less concave than that of the current

river (Figures 4A and B). Related stream gradients are 0.011 m/m for the current situation and 0.015 m/m for the past.

Modern river belt widths vary from 25 m to 350 m over the entire reach. Between the coast and 50 km from the coast, the river belt is unconfined and >150 m wide. Farther upstream, the river belt is confined to a 50-150 m-wide section (Figure 6A), which yields a mean value of 75±15 m.

During Minchin times, river belt width values varied between 400 and 800 m (mean value 550±100 m) at >50 km upstream distance of the Pacific coast, and c. 1000 m farther downstream (Figure 6B). As outlined above, the modern situation revealed that widths of active channels are nearly constant along the entire Pisco River (for both low and high water stages), and that related values correspond to between 1/3 and 2/3 of the river belt width values that we encountered upstream of the gauging station. These considerations return active channel width values that range between c. 150 and 210 m for low water stages, and c. 300-420 m for high discharge situations.

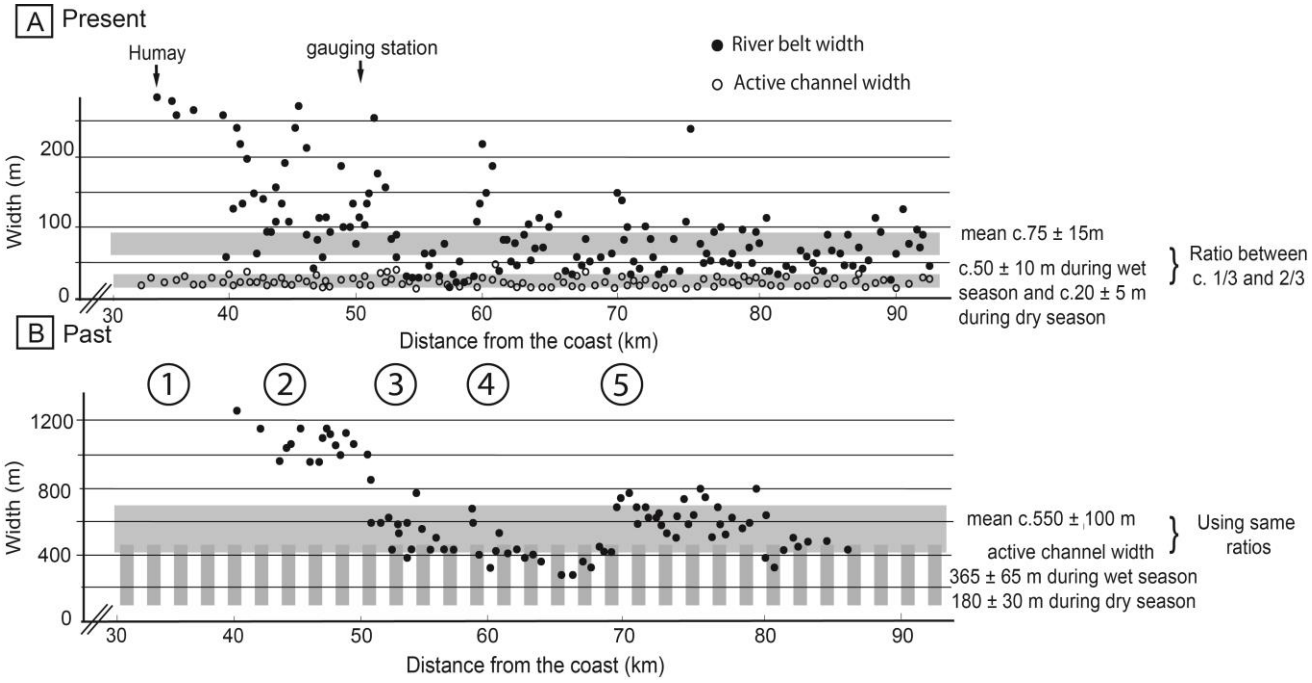

Figure 6: *(A) River belt and active river channel widths along the Pisco River from the Pacific coast to 100 km distance from the coast during the modern time. This yields a ratio between river belt and active channel widths ranging between 1/3 and 2/3. (B) River belt width and estimation of active channel width during the Minchin time using the same ratio between these variables as to the present situation.*

Grain size data

River grain size variation is an important property of streams controlled by the magnitude of the water discharge (e.g. Duller et al., 2012). In our case, the D_{50} varies between 0.8 and 3.6 cm, and between 1.9 and 3.7 cm for the modern and the Minchin deposits, respectively (Figure 7A). In the same sense, the D_{96} varies between 4.5 and 9.5 cm for the present material, and 8.7 and 18.4 cm for the past deposits (Figure 7B). At all sites, the ancient material is coarser for the two percentiles than the present material. Likewise, the modern bed material is better sorted than the Minchin deposits, i.e. D_{96}-D_{50} ~ 10.5 cm for the Minchin deposits compared to D_{96}-D_{50} ~ 4.8 cm for the modern bed material. In addition, the Minchin deposits are characterized by the occurrence of 2-3 m-large boulders particularly at upstream sites (Figure 2B). In contrast, meter-sized boulders are nearly absent

in the modern river bars, and the material appears more homogenous in terms of granulometric composition (Figure 2F).

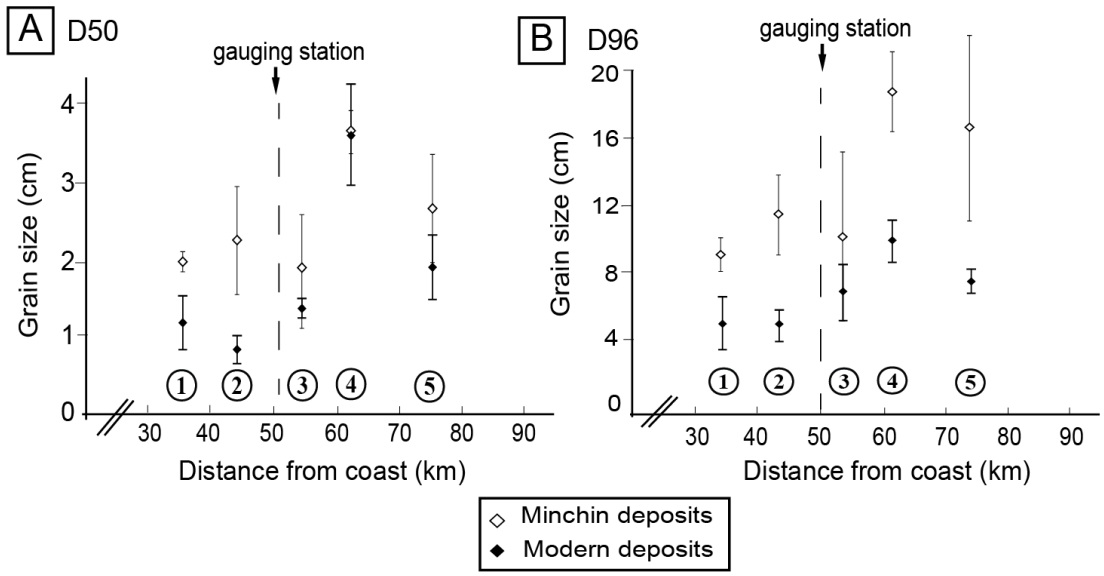

Grain sizes of modern and Minchin deposits against distance from the Pacific coast. The black diamonds represent the modern deposits and open diamonds represent the Minchin material. The vertical bars correspond to the grain size standard deviation between the photographs at each site. Note changes in scale on y-axis.

Water discharge estimates for the modern situation

The combination of information about grain size, river morphology and sediment discharge allows the calculation of modern and paleo water discharges. Using the Bagnold relationships between sediment discharge and water flow strength (Equation 1), we obtained the shear stress and the related water flux required to mobilize the supplied sediment under the condition that flow strengths exceed critical values to entrain the D_{50} and D_{96} (see methodology).

For the modern scenario a mean water discharge of 2.5 m^3/s (row labeled with *mean* in Table 1). This was based on a value of the constant in the Bagnold equation of a = 1 and average parameter values of 1.1 cm for D_{50} and 20 m for the active channel width. We note that a value of 2.5 m^3/s is up to 10 times less than the mean water flux measured at the gauging station. The constant in the Bagnold equation thus needs to be adjusted to *a=1/20* to achieve the known mean discharge value of c. 25 m^3/s. Minimum and maximum values of channel widths and D_{50} return water discharge estimates between 1 and 4 m^3/s (a=1) and 15-35 m^3/s (a=1/20) (Table 1). In summary, these results represent estimates of flow strengths, which would be required to evacuate the supplied sediment Q_s (Table 1) under the condition that the D_{50} sets the threshold for the entrainment of the sediment.

Also for the modern situation, the use of (Table 1): 7.5 cm for the D_{96}, 50 m for the channel width, and 0.045 for the Shields criterion for the entrainment of sediment returns an average water discharge of 40 m^3/s during floods, provided that *a=1*. This is c. 1.5 times less than the annual mean of maximum runoff that has been measured. A corresponding adjustment of the constant in the Bagnold equation to *a=1/5* allows to correct for this underestimate (row labeled as *mean* in Table 1). The consideration of minimum and maximum values for channel widths, the D_{96} and Shields criterion runoff values between 12 and 100 m^3/s (a=1) and 18-150 m^3/s (a=1/5) (Table 1). These represent estimates for the present maximum water discharge, which would be required to evacuate the supplied sediment Q_s (Table 1), provided that the D_{96} sets the threshold for the entrainment of the sediment.

Water discharge estimates for Minchin times

We proceeded in the same way as for the modern situation, but used the calibrated model where a=1/20 if the D_{50} sets the threshold conditions for sediment transfer, or alternatively a=1/5 if the D_{96} is considered (see also equation 1). Accordingly, for Minchin times, the use of mean values including: (i) 2 cm for the D_{50} as threshold percentile for the transport of sediment, (ii) 180 m for the active channel width, and (iii) 227000 m^3/s for sediment discharge returns a mean runoff value of 180 m^3/s for the past (row labeled as *mean* on Table 2), which is 7 times larger than what is currently being measured. The consideration of minimum and maximum values for channel widths and the D_{50} plus the full range of sediment discharge estimates returns water runoff values between 70-300 m^3/s (Table 2).

In the same sense, the use of mean values for the parameters that we related to peak water discharge such as (row labeled as mean on Table 2): (i) 12 cm for the D_{96}, (ii) 365 m for the channel width, (iii) 0.045 for the Shields criterion for the entrainment of sediment, and (iv) 227000 m^3/s for sediment discharge returns a mean water discharge estimate of 490 m^3/s that is required to evacuate the sediment (Table 2). This is c. 3 times larger than the inferred mean discharge value during Minchin times and 8 times larger than the corresponding mean discharge values that is currently being measured during peak conditions. The consideration of minimum and maximum values for channel widths, the D_{96} and Shields criterion and the full range of sediment flux returns water discharge values between 130 and 1300 m^3/s.

Interpretation and discussion

Data about the river morphology, the downstream grain size characteristics and the estimated water flux are used to infer the sediment transport dynamics in the Pisco River for the two studied time periods. We first present a section that discusses the validity of the selected models. In the subsequent sections, we will use our results to infer: (i) the timescales of sediment transport, (ii) contrasts in discharges between the present and the past, and (iii) implications from the difference in the sorting between modern and past times.

Selected Model

The use of a =1 in the Bagnold equation (1) returns discharge values that are between 10 and 1.5 times lower than the measured ones if the mean and maximum flood stages are considered, respectively (Figure 8). Corrections where we set a ≈ 1/20 and a ≈ 1/5 yield discharge estimates that closely correspond to the measured runoff during low and maximum water stages, respectively. As the Bagnold equation for sediment transport is based on the concept that sediment flux is accomplished in response to the ratio between drag and inertia forces, the 4 times larger value for the constant *a* during peak discharge (compared to low runoff stages) implies that during high discharge events, drag forces are more efficiently transferred into transport work than during low water stages. Related effects are also implied by the *Variable-Power Equations* of Ferguson (2007), where the friction factor *f* is inversely related to the water depth relative to the particles' grain sizes. Additionally, the contrasts in the assigned values for *a* (Bagnold equation 1) during low and high discharge are in nearly the same range as the ratios of the coefficients a_1 and a_2 of the *VPE*-approach (equation 7) that scale the conditions during high and low flows, respectively.

However, our simple sensitivity analyses shows that the largest uncertainties in our model are related to channel gradient, *S,* where a doubling or halving of this variable requires the water discharge variable to be adjusted by a factor of 4 to maintain the same sediment transport rate (Table 1). Doubling or halving of channel width affects discharge estimates by a factor of 1.5, while doubling or halving the mean grain size value affects discharge estimates by a factor of 3.

We also note that our model is set up such as that the transport work of the Pisco River can be accomplished on an annual basis. While this assumption is sustained by other studies (Emmett and Wolman, 2001; van der Berg and Schlunegger, 2012), some authors proposed that most of the erosional and transport work of streams is accomplished by large floods with long return intervals. These latter findings are based on observations in the USA and contrasts between ^{10}Be-based denudation rates and decadal sediment yields in the European Alps (e.g, Molnar, 2001; Wittmann et al., 2007). While we cannot properly determine the time span required to transfer the sediment in the Pisco River with the current dataset, we tentatively favor a model where most of the sediment transport is accomplished during short time intervals spanning a few years at most.

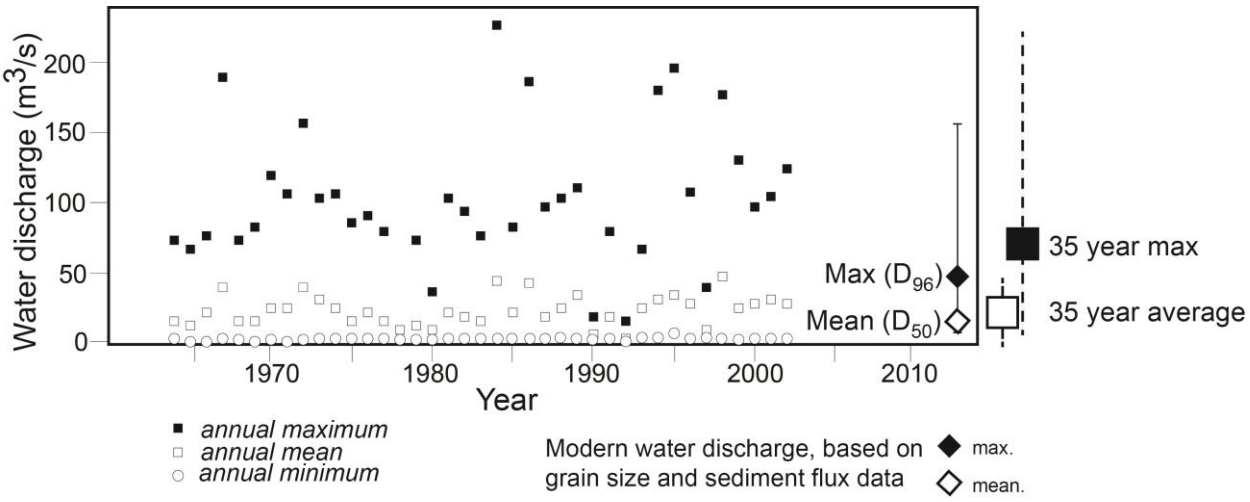

Figure 8: *Recorded water discharge in the Pisco River, collected at the gauging station (modified after Bekaddour et al., 2014). Annual water discharge estimated from grain size and sediment flux data are presented by the diamond symbols.*

Differences in inferred discharge patterns during the past and modern times

The analysis presented here demonstrates that water discharge of the Pisco River during Minchin times was larger than that of the modern Pisco River. This result mainly reflects the coarser grain size distribution of the Minchin-age terrace deposits (e.g. Figure 2B), which is also supported by ^{10}Be-based sediment flux calculations for the Minchin period (Bekaddour et al., 2014). Potential errors to the analysis are introduced through an overestimation of channel widths and the introduction of coarser particles through debris flow processes. With regards to channel width, we are confident in our estimates of channel width as they are based on conservative grounds. With regards to the contribution of coarser particles through debris flow processes, this might explain the occurrence of m-scale boulders in the upper reaches but, we stress that these boulders are embedded within fluvial gravels and so must have been transported by the Pisco River (Steffen et al., 2009). Furthermore, the terrace material along the lowermost reaches of the Pisco River is composed of fluvial gravels, and debris flow-derived material occurs only as thin units that are of limited lateral extent and constrained to the hillslope borders and tributary valleys.

We note, however, that the inferred difference in water discharge could be biased since the sediment supply exerts an important influence on bed grain size in modern channels (e.g., Buffington and Montgomery, 1997). In particular, the terrace deposits are by definition from a non-equilibrium period in the channel's history when sediment supply was higher than transport capacity. Accordingly, the grain size of the paleo-supply could be quite different from the modern conditions, which then requires that inversions of our equations for water discharge needs the consideration of

changes in sediment supply and related grain size through time. In a similar context, Krumbein and Lieblein (1956) showed that most of the anomalously large particles in gravel deposits are probably normal members of the stream particle population. However the larger value of graphical standard deviation of the Minchin deposits compared to the modern is suggestive of a true causative mechanism, which we infer to be driven by the hydraulic regime of the river system (Manville and White, 2003). We are currently not able to properly solve this problem, but we note that our inference of larger discharge values not only relies on the grain size data, but also on the contrasts of supplied and evacuated sediment (Bekaddour et al., 2014), which we did consider through the application of equation 1. Accordingly, the interpretation of larger discharge values and a wetter climate for the past will not change.

Implications from the difference in the sorting

The poorer sorting of the Minchin material might reflect that the past was characterized by a larger divergence from equal mobility, when the timescale of rapid transient events was too short, or shorter than today, to allow equilibration to equal mobility (Miller et al., 2014). This concept has been used to explain the dependency of downstream fining rates on the threshold of motion (e.g., Miller et al., 2014) and the rapid supply of coarse-grained material with a poor initial sorting (e.g., Manville and White, 2003). Indeed, a larger divergence from equal mobility could have been accomplished by a high relative importance of sediment supply through erosion on the valley borders, versus sediment evacuation in the channel, which likewise points to a relatively high sediment discharge/water flux ratio. We are currently not able to test this latter hypothesis, but the occurrence of sediment accumulation during Minchin times (Steffen et al., 2009) and ^{10}Be-based large sediment supply rates from bordering hillslopes (Bekaddour et al., 2014) do support this argument.

Summary and Conclusions

Terrace successions in the Pisco Valley, Peru have been used to infer a climatic (Steffen et al., 2009), specifically a wetter climate (Bekaddour et al., 2014) origin, without a physically-based dataset to reinforce this assertion. Using sedimentological and morphometric parameters of the Minchin terrace succession, we were able to reconstruct the paleo-water discharge during the Minchin time interval. Using the 50th and 96th percentile fractions of the grain size distributions to denote mean water discharge and maximum water discharge, we find that the Pisco River, during Minchin times, was characterized by a larger discharge (Figure 9), which was c. 7-8 times greater than today. In this context, an increase in the mean and maximum water discharge could either be related to a wetter climate along the Pacific coast as postulated by Bekaddour et al. (2014), or to high precipitation rates on the Altiplano (Baker et al., 2001a, b), or to a combination of both. We note, however, that we are currently not able to distinguish between both scenarios with the here presented dataset.

In summary, by linking grain size and morphometric data of the modern Pisco River to measured water discharges over the past 60 years, we calibrate our paleo-hydrological investigation of the Minchin-age succession. This, combined with chronology and sediment flux data from ^{10}Be, illustrates that the dynamics of a river system can be deciphered with a reasonable degree of confidence from high-resolution sedimentological and morphometric dataset.

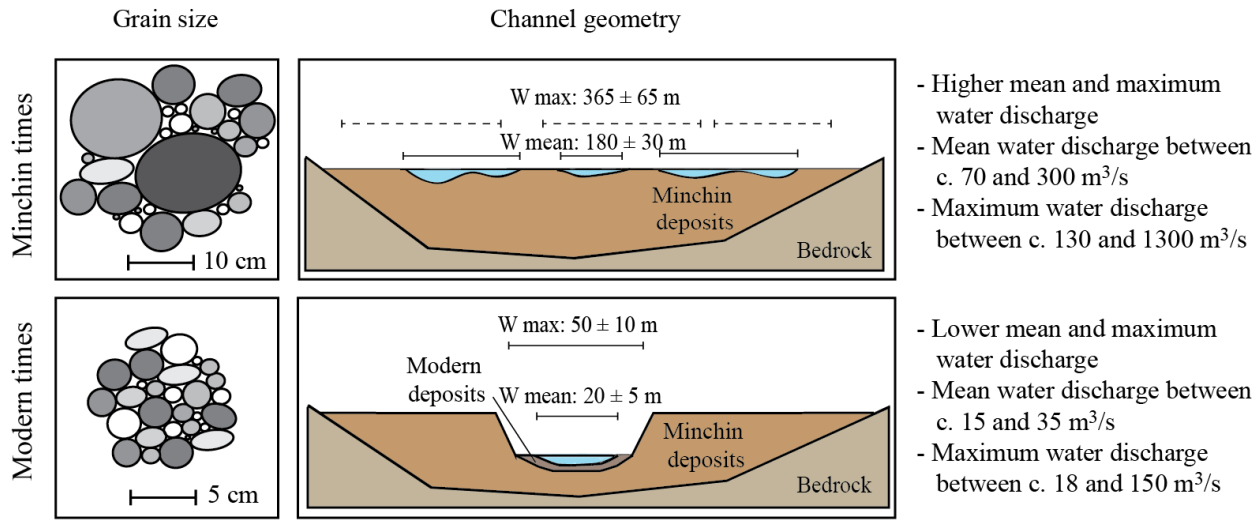

Figure 9: *Summary figure illustrating grain size patterns, channel properties and hydrological conditions during modern and Minchin times.*

Acknowledgments

This project originates from the first author's doctoral work. It is funded by the Swiss National Science Foundation (project Number 137516). We greatly acknowledge Naki Akçar for field assistance. The constructive comments and suggestions by the associate and chief editors substantially improved the science and clarity of the paper.

References

Abbühl, L. M., Norton, K. P., Jansen, J. D., Schlunegger, F., Aldahan, A. and Possnert, G., 2011. Erosion rates and mechanisms of knickzone retreat inferred from 10Be measured across strong climate gradients on the northern and central Andes Western escarpment. Earth Surf. Process. Landf. 36, 1464–1473.

Agteca, 2010. Global Historical Climatology Network (GHCN-Monthly database) compilation for Peru edited. Cochrane, T.A., Agteca.org.

Andrews, E. D., 1983. Entrainment of gravel from naturally sorted riverbed material. GSA Bulletin 94, 1225-1231.

Andrews, E. D., 1984. Bed material entrainment and hydraulic geometry of gravel-bed rivers in Colorado. Bull. Geol. Soc. Am. 95, 371-378.

Allen, P. A., 2008. From landscapes into geological history, Nature, 451, 274–276.

Baker, P. A., Seltzer, G. O., Fritz, S. C., Dunbar, R. B., Grove, M. J., Tapia, P. M., Cross, S. L., Rowe, H. D. and Broda, J. P., 2001a. The history of South American tropical precipitation for the past 25,000 years. Science 291, 640–643.

Baker, P. A., Rigsby, C. A., Seltzer, G. O., Fritz, S. C., Lowenstein, T., Bacher, N.and Veliz, C., 2001b. Tropical climate changes at millennial and orbital timescales on the Bolivian Altiplano. Nature 409, 698–701.

Bekaddour, T., Schlunegger, F., Vogel, H., Delunel, R., Norton, K. P., Akcar, N.and Kubik, P., 2014. Paleo erosion rates and climate shifts recorded by Quaternary cut-and-fill sequences in the Pisco valley, central Peru. Earth and Planetary Science Letters 390, 103-115.

Buffington, J. M. and Montgomery, D. R. 1997. A systematic analysis of eight decades of incipient motion studies, with special reference to gravel-bedded rivers. Water Resources Research, 33, 1993–2029.

Church, M., 2002. Geomorphic thresholds in riverine landscapes. Freshwater Biology, 47, 541-557.

Church, M., 2006. Bed material transport and the morphology of alluvial river channels. Annal Reviews of Earth and Planetary Science Letters, 34, 325-354.

Davila, F. M., 1993. Geología de los cuadrángulos de Pisco, Guadalupe, Punta Grande, Ica y Cordova: Lima, Perú. Instituto Geológico Minero y Metalúrgico boletín. 47-62.

Diplas, P. and Fripp, J., 1991. Bed material sampling: issues and answers. In Proceedings of the Fifth Federal Interagency Sedimentation Conference, Las Vegas, Nev, 2-81.

Duller, R. A., Whittaker, A. C., Swinehart, J. B., Armitage, J. J., Sinclair, H. D., Bair, A. and Allen, P. A., 2012. Abrupt landscape change post-6 Ma on the central Great Plains, USA. Geology 40, 871-874, doi: 10.1130/G32919.1.

Egiazaroff, I.V., 1965. Calculation of nonuniform sediment concentrations. Journal of Hydraulic Engineering, 91, 225–247.

Emmett, W. W. and Wolman, M. G., 2001. Effective discharge and gravel bed rivers. Earth Surface Processes and Landforms, 26,1369-1380.

Ferguson, R, 2007. Flow resistance equations for gravel- and boulder-bed streams. Water Resour. Res., 43, W05427.

Heller, P. L., and Paola, C., 1992. The large-scale dynamics of grain size variation in alluvial basins: 2. Application to syntectonic conglomerate. Basin Res., 4, 91–102.

Hinderer, M., Kastowski, M., Kamelger, A., Bartolini, C. and Schlunegger, F., 2014. River loads and modern denudation of the Alps, A review, Earth-Science Reviews, v. 118, p. 11–44

Humphrey, N. F. and Heller, P. L., 1995. Natural oscillations in coupled geomorphic systems: An alternative origin for cyclic sedimentation. Geology, 23, 499-502.

INGEMENT: Instituto Geologico Minero y Metalurgico de Peru, 2011. Geologia Nacional Geocatmin version 1.5.1, Capa 12. Lima, Peru.

Jarrett, R. D., 1984. Hydraulics of high gradient streams. ASCE J. Hydraul. Eng., 110, 1519–1539.

Kellerhals, R. and Bray, D.I., 1971. Sampling procedures for coarse fluvial sediments. Journal of the Hydraulics Division, 97(8), 1165-1180.

Krumbein, W. C. and Lieblein, J., 1956. Geological application of extreme-value methods to interpretation of cobbles and boulders in gravel deposits. Eos, Transactions American Geophysical Union, 37(3), 313-319.

NASA Land Processes Distributed Active Archive Center (LP DAAC). ASTER GDEM. USGS/Earth Resources Observation and Science (EROS) Center, Sioux Falls, South Dakota, 2001.

Manville, V. and White, J. D. L., 2003. Incipient granular mass flows at the base of sediment-laden floods, and the roles of flow competence and flow capacity in the deposition of stratified bouldery sands. Sedimentary Geology 155, 157–173.

Marcus, W. A., Leslie Harvey, K. R. and Tackman, G., 1992. An evaluation of methods for estimating Manning's n in small mountain streams. Mountain Research and Development 12, 227–239.

McPhillips, D., Biermann, P. R., Crocker, T. and Rood, D. H., 2013. Landscape response to Pleistocene–Holocene precipitation change in the Western Cordillera, Peru: 10Be concentrations in modern sediments and terrace fills. J. Geophys. Res., Earth Surf. 118, 1–12.

McPhillips, D., Biermann, P. R. and Rood, D. H., 2014. Landslide erosion in the Andes likely triggered by earthquakes not precipitation. Nat. Geosci., 7, 927-930.

Meyer-Peter, E., and Müller, R., 1948, June. Formulas for bed-load transport. Hydraulic Structures Research, 39-64.

Miller, K. L., Reitz, M. D. and Jerolmack, D. J., 2014. Generalized sorting profile of alluvial fans, Geophys. Res. Lett., 41, 7191–7199, doi:10.1002/2014GL060991.

Molnar, P., 2001. Climate change, flooding in arid environments, and erosion rates, Geology, 29, 1071–1074.

Parker, G., Klingeman P.C., McLean D.G., 1982. Bedload and size distribution in paved gravel-bed streams. J. Hydraul. Div. Am. Soc. Civ. Eng., 108, 544–571.

Placzek, C., Quade, J. and Patchett, P. J., 2006. Geochronology and stratigraphy of late Pleistocene lake cycles on the southern Bolivian Altiplano: implications for causes of tropical climate change. Geol. Soc. Am. Bull. 118, 515–532.

Rice, S. and Church, M., 1998. Grain size along two gravel-bed rivers: statistical variation, spatial patterns and sedimentary links. Earth Surf. Process. Landf., 23, 345-363.

Ryder, J. M. and Church, M. 1986. The Lillooet terraces of Fraser River: a palaeoenvironmental enquiry. Canadian Journal of Earth Sciences, 23(6), 869-884.

Shields, A., 1936. Anwendung der Ahnlichkeitsmekanik und der Turbulenzforschung auf die Geschiebebewegung, Mittelung der preussischen Versuchsanstalt fur Wasserbau und Schiffbau, 26. (Berlin).

Schildgen, T. F., Hodges, K. V., Whipple, K. X., Reiners, P. W. and Pringle, M. S., 2007. Uplift of the western margin of the Andean plateau revealed from canyon incision history, southern Peru. Geology 35, 523–526.

Schlunegger, F. and Hinderer, M., 2003. Pleistocene/Holocene climate change, re-establishment of fluvial drainage network and increase in relief in the Swiss Alps. Terra Nova, v. 2, p. 88-95

Steffen, D., Schlunegger, F. and Preusser, F., 2009. Drainage basin response to climate change in the Pisco valley, Peru. Geology 37, 491-494.

Trauerstein, M., Lowick, S. E., Preusser, F. and Schlunegger, F., 2014. Small aliquot and single grain IRSL and post-IR IRSL dating of fluvial and alluvial sediments from the Pativilca valley, Peru. Quatern. Geochronol. doi.org/10.1016/j.quageo.2013.12.004.

Tucker, G. E. and Slingerland, R., 1997. Drainage basin response to climate change. Water Resour. Res. 33, 2031–2047.

Van den Berg, J., and Schlunegger, F., 2012. Alluvial cover dynamics in response to floods of various magnitudes: The effect of the release of glaciogenic material in a Swiss Alpine catchment. Geomorphology, 141-142, 121-133.

Von Blanckenburg, F., 2005. The control mechanisms of erosion and weathering at basin scale from cosmogenic nuclides in river sediment. Earth and Planetary Science Letters, 237(3), 462-479.

Whipple, K. X., 2004. Bedrock rivers and the geomorphology of active orogens. Annu. Rev. Earth Planet. Sci., 32, 151-185.

Whittaker, A. C., Attal, M. and Allen, P.A., 2010. Characterising the origin, nature and fate of sediment exported from catchment perturbed by active tectonics. Basin Research. 22. 809-828.

Wittmann, H., von Blanckenburg, F., Kruesmann, T., Norton, K. P. and Kubik, P. W., 2007. Relation between rock uplift and denudation from cosmogenic nuclides in river sediment in the Central Alps of Switzerland. Journal of Geophysical Research: Earth Surface, 112.